ADVANCED MATERIALS
www.advmat.de

3D Imaging of Ferroelectric Kinetics during Electrically Driven Switching

Mousa Ayoub, Hannes Futterlieb, Jörg Imbrock, and Cornelia Denz*

The dynamics of ferroelectrics, especially of those which show relaxor behavior, have been a long-standing puzzle. Different theoretical models have been discussed in the literature to describe the domain kinetics in the relaxor regime.[1–11] In general, the efforts devoted to modeling the dynamics of the ferroelectrics lack a 3D visualization of the growth or switching events. Even those combined with domain imaging are suffering from different disadvantages, which may have an impact on the studied case. Many of them are destructive measurements and cannot be used to acquire real-time or in situ information about the ferroelectric kinetics, as for instance selective chemical etching.[12] Chemical etching is still the most widely utilized method, even though it is restricted to 2D. Different methods are designed to be nondestructive, like optical methods which are used for in situ measurements and considered as the most informative and convenient methods, such as toning,[13] interferometry,[14] near-field optical microscopy,[15] electrooptic imaging,[16,17] confocal frequency doubling,[18] Raman spectroscopy,[19] optical coherence tomography,[20] and nonlinear Talbot imaging.[21] All these optical methods belong to the 2D steady-state studies, which cannot record dynamics in the volume. Moreover, successful 3D imaging measurements of domain structures have been made using second-harmonic generation microscopy. However, domain imaging in the volume of ferroelectric crystals using conventional second-harmonic generation (SHG) microscopy is restricted to a certain wavelength regime, and up to now only static domain formations have been imaged.[22–25] Recently, an optical technique based on a noncollinear phase-matching condition, called Čerenkov SHG microscopy has been established.[26,27] With this technique it is possible to image ferroelectric domains in 3D.

Polarization reversal is considered as an example of ferroelectric kinetics or phase transformation process.[28–30] These have much in common with such well-known phenomena as switching in ferromagnetics and liquid crystals. To date several attempts have been made to measure the kinetics of the spontaneous polarization,[31–33] using for example electron microscopy (SEM and TEM), nematic liquid crystals and pyroelectric probe scanning.[34–36] In this context, a unique experiment to record this process in pseudo 3D has been made, meaning in only two spatial dimensions and time as the third dimension,[37] which is typically considered as $(2d + 1)$ dynamics. 3D surface polarization topography of thin films can be offered with a resolution of few nanometers using piezo force microscopy (PFM).[38,39] This method belongs however to the steady state methods and cannot visualize different polarization states in a crystal volume as deep as Čerenkov-type SHG microscopy.[26,27] Thus, no spatial dynamically resolved 3D imaging of this important process in bulk material was possible. Here we propose to combine Čerenkov-type SHG microscopy with recording of transient current, which is considered the most popular experimental method of studying the polarization reversal. The current represents the integrated response of the system and is formed by a large number of ferroelectric domains arising and growing during switching.[28] The characteristic transient current explains the sideways and forward domain wall motion phenomenologically.[40] From the current, one can then easily calculate the hysteresis loop, by integrating the current over time. Čerenkov-type SHG microscopy is a modern technique to directly detect $\chi^{(2)}$ boundaries, e.g., between inverted ferroelectric domains, with a sub-micrometer accuracy over the whole crystal depth. However, the absolute orientation of the polarization of an individual domain cannot be deduced. For this, charge sensitive methods as PFM can be used at the surface. Čerenkov-type SHG is based on the generation of second harmonic noncollinearly to the fundamental beam. For this scheme only the longitudinal phase-matching condition is satisfied.[41–43] Consequently, SH signals are expected to be emitted transversely under a defined angle. This concept differs from that used in the conventional second-harmonic generation microscopy,[22,24,25] in which the phase mismatch Δk has to be less than zero for second-harmonic generation in the forward direction only. The emission angle between the second harmonic and fundamental beam in Čerenkov-type SHG is derived on the basis of the longitudinal phase-matching condition $\cos\theta = 2k_1/k_2$. Here, k_1 and k_2 are the wave vectors of the fundamental and the SH beams, respectively. This remarkable kind of harmonics generation has been recently used for characterization of nonlinear photonic structures in 3D.[38,39,44]

For the aim of this paper we employ a ferroelectric single crystal with a simple domain structure, i.e., a uniaxial ferroelectric with relatively low coercive field and experimentally convenient temperature region of the ferroelectric phase: strontium barium niobate (SBN). SBN is a relaxor ferroelectric material, possesses 180° needlelike domain structures along the crystal's polar axis and shows fractal-like pattern with a wide length scale at the polar-end faces.[45–47] These patterns exhibit an irregular spatial distribution because of the random domain size. The individual domains have the form of rods or pyramids with a quadratic shape, corresponding to the crystal symmetry 4 mm.[23,48] The reported domain widths in SBN

Dr. M. Ayoub, H. Futterlieb,
Dr. J. Imbrock, Prof. C. Denz
Institute of Applied Physics
Westfälische Wilhelms-Universität Münster
Corrensstraße 2/4, 48149 Münster, Germany
E-mail: ayoubm@uni-muenster.de

DOI: 10.1002/adma.201603325

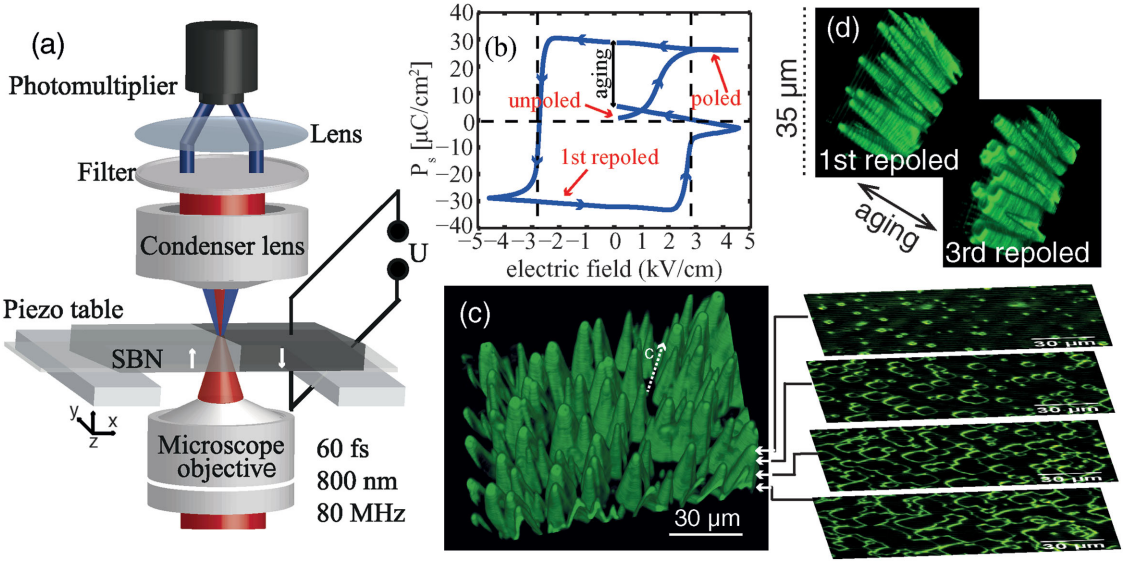

Figure 1. a) Experimental configuration used for laser scanning Čerenkov second-harmonic microscopy (ČSHM). b) The characteristic *P*–*E* loop of relaxor SBN. c) A 3D image taken by ČSHM of microscaled needlelike ferroelectric domains in SBN crystal. Four 2D slices of (c) at different depths. d) Two 3D images at different poling states showing the aging effect. Green lines represent domain walls, i.e., they separate regions of polarizations with opposite orientation pointing either upward or downward. The polarization inside the green pyramids in (c) points in one direction along the *c*-axis and the polarization outside the green pyramids points in the opposite direction.

crystals range between a few hundred nanometers and a few micrometers.[49–52]

In the following, the experimental procedure of monitoring the domain kinetics will be explained. This is categorized with respect to the poling state of the studied volume (see Experimental Section).

The experimental procedure is realized as follows: We commence our systematic investigation with an unpoled sample. Then, the sample is poled at room temperature by applying an external electric field stepwise until finally 4 kV cm^{-1} is reached. The step size is about 0.15 kV cm^{-1}. This is fixed in all poling and repoling experiments. The poled sample is mounted and sandwiched between two cover-slips coated with indium tin oxide (ITO) films under the microscope. While increasing the electric field, a 3D space of $40 \times 60 \times 60$ μm^3 is scanned layer by layer at different depths in the sample and the poling current is recorded (see example in **Figure 1**c). We will extract the domain walls from each layer at each electric field.

In the first repoling, a nucleation process is expected to happen in volume. Similar to any first-order phase transition and beginning from nuclei as seeds, new ferroelectric domains arise in random places at different depths in the crystal during phase transition.

The probability of accruing nucleation is ruled by the distribution of the crystal lattice imperfections.[27] After that the new domains start growing, i.e., their walls move in all possible space directions. Thus the switching process is described as the growing of already existing domains. Because we apply slow field ramps the time dependence of nucleation probability has not been considered here. We note that the applied ramp is very slow in order to be able to scan a 3D volume. Slower ramps would make it possible scanning larger volume. In contrast, faster ramps reduce the scanned volume, and thus the collected data.

A sequence of the development in this phase is depicted in **Figure 2** (see Video S1, Supporting Information). Starting with the poled case, we chose a volume of $40 \times 60 \times 60$ μm^3 in which no domain walls are visible in order to ensure the maximum contrast. To distinguish the event of domain formation from the noise signal, we did not diminish the background signal. Thus, for 0 kV cm^{-1}, only a background signal is measured (Figure 2a), which corresponds to a complete absence of any domain walls. The measurement is then started by increasing the external applied field and simultaneously measuring the current (Figure 2j). After each increasing step of the electric field, the same volume was scanned. The imaging shows no domain walls with increasing electric field until about 2 kV cm^{-1}. No current flowed in this range and only the noise signal was measured. Thus the chosen scanned space is sufficient as a representation of the whole sample. If the field is increased further, the current starts flowing. Nanoscaled domains arise, referring to the nucleation process (Figure 2b). As soon as the domain walls appear, the noise signal disappears, because the SHG signal is much stronger than the background noise. Each layer in which only a homogenous background is visible is completely free of domain walls, as mentioned above. More domains arise and the existing domains grow mainly in length while increasing the electric field, but less pronounced growth in the lateral direction is also observed (Figure 2d,e). It is also interesting to note that the ferroelectric domains take their characteristic form, namely a square with rounded corners, directly at the first flank of the characteristic current peak. This individual domain shape is determined by the crystal symmetry 4 mm and elastic properties.[53] Note that this optical method does not determine the direction of the spontaneous polarization, even though one can easily conclude that the polarization surrounded by the domain walls is antiparallel to the polarization outside. The direction is determined by the sign of the flowing current. By further

Adv. Mater. **2016**,
DOI: 10.1002/adma.201603325

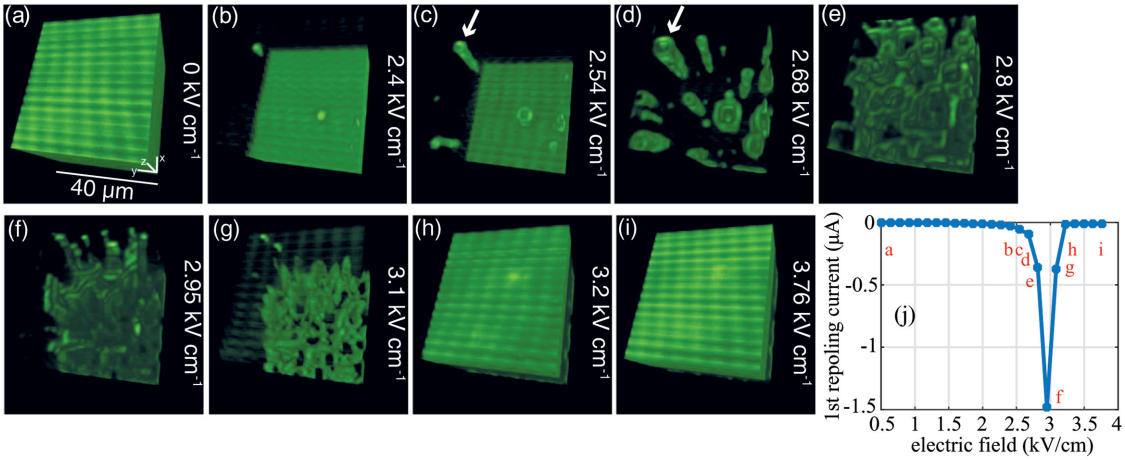

Figure 2. a–i) Measured 3D sequence of the first repoling process of a SBN crystal. The arrow points to a growing domain. j) The images are labeled on the corresponding transient current and the intensity in each image is normalized to its maximum value, i.e., the amplitude of the background noise in (a), (b), (h), and (i) is much lower than the signals from the domain walls in (b)–(g). Green lines represent domain walls (see Video S1, Supporting Information).

increasing the field, new domains arise and the large domains grow further until the turning point of the current peak, at which the most pronounced process is the lateral motion of the domain walls, i.e., the antiparallel polarization begins to become dominant at the expense of the parallel polarization direction. The domains grow further with increased field strength, and the domains merge. The domain walls consequently vanish again, as the noise signal returns (Figure 2f–h). In this and the following measurements we observe the growth of the homogenous region in the direction of the *c*-axis. One notes that from this point on no current is flowing and no further events are recorded. However, the scanned crystal volume is not perfectly switched and at the bottom of the scanned space domain walls can still be observed (Figure 2h,i). This explains the aging behavior of the hysteresis loop (Figure 1b), i.e., the reason why the loop shrinks. The measurements also allow us to determine the growing rate of the individual domains with high accuracy in the depth over several tens of micrometers. An example is depicted in **Figure 3**. In Figure 3, the transverse and the longitudinal growth of a domain, which is marked in Figure 2 c,d, are plotted in dependence of the applied voltage. The domain is measured from 2.4 kV cm^{-1}, i.e., the field at which it arises

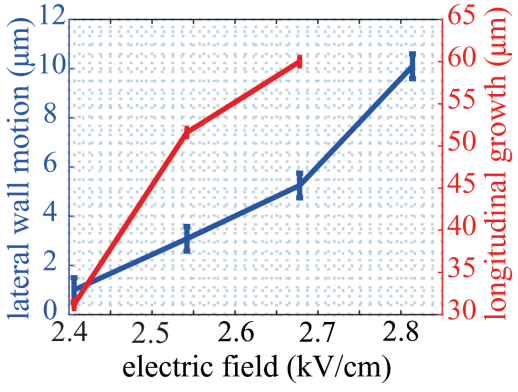

Figure 3. The growth rate of the domain marked in Figure 2c,d showing the lateral and longitudinal growth in dependence of the applied field.

up to 2.8 kV cm^{-1}, where it merges with other domains. The domain size increases with increasing applied field from 1 μm (resolution limit) to about 10 μm. One clearly sees that the domain grows faster in the length than in the lateral direction. It reaches 60 μm already at 2.6 kV cm^{-1}.

Furthermore, the origin of the characteristic domain shape in the depth is determined.

Figure 4 shows 2D images at different depths "z_i" extracted from the volume shown in Figure 2d at the field strength 2.68 kV cm^{-1}, where "z_i" is the depth at which the volume is recorded. A schematic illustrating the domain shape formation with the height is depicted in Figure 4f. Four nanoscaled domains form the origin of the 4 mm symmetric shape. The image series illustrates the decreasing of the domain diameter from about 8 μm at "z_i" (Figure 4a) to smaller than 1 μm at "z_i + 45 μm" (Figure 4e). The clear formation of the individual domain shape becomes very apparent. The fourfold symmetry shown in Figure 4a originates from four nanoscaled domains, from which the domain starts to grow (Figure 4e). These are easily distinguishable in Figure 4b. These build a symmetric fourfold cluster, proving that the expansion rate is the same one for both *x* and *y* directions, unlike to 3m symmetric materials as $LiNbO_3$, where the expansion rate is laterally different and leads therefore to triangles or hexagons. Figure 4d,e shows the resolution limit of our microscope. Consequently, the four domains seem to be not fully separated and the walls overlay in the center of the structure, giving a form of a cross. The signal intensity is stronger in the center of the cross.

In the second repoling, we aim to study the growth and switching of available domains. **Figure 5** shows the sequence of the second repoling process and its corresponding current (see Video S2, Supporting Information). We start repoling the sample from the state labeled in (Figure 2i). Unlike the first process, changes are observed at much smaller electric fields. The remaining domain walls start to grow again and the noise diminishes gradually (Figure 5b,c). The domains grow vertically and antiparallel to the first repoling process (Figure 2b,c). Further increase of the field shows more complex behavior of the growing process. Since the domains are growing from

ADVANCED MATERIALS
www.advmat.de

Materials Views
www.MaterialsViews.com

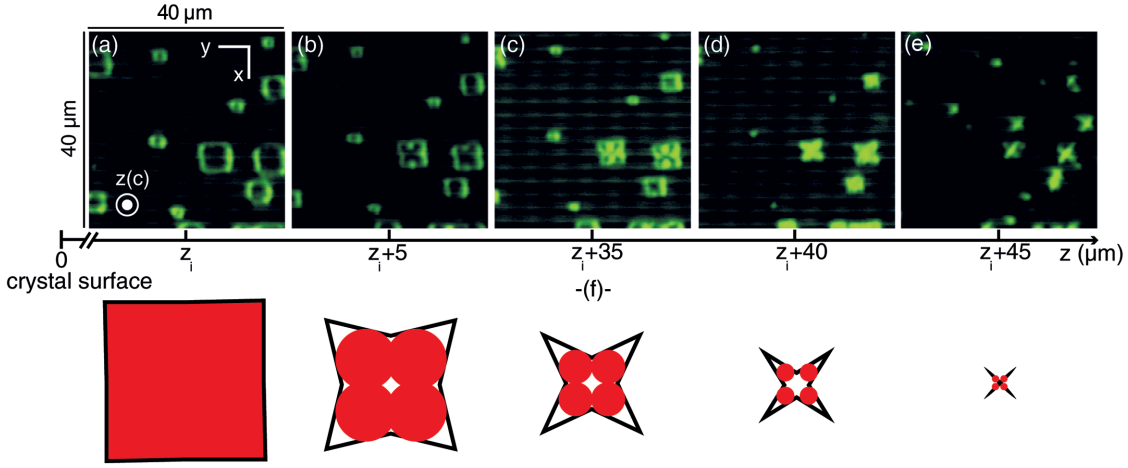

Figure 4. a–e) 2D images at different depths "z_i" extracted from the volume shown in Figure 2d at the field strength 2.68 kV cm^{-1} during the first repoling process. f) Diagram illustrating the evolution of the fourfold symmetry of the domain shape in dependence of depth observed experimentally.

already existing clusters (Figure 5e,h), the second repoling process shows a more complex growing process than the first one, where the domains were growing from strewn nuclei. Nevertheless, the dynamics still feature the characteristic wall motions, i.e., first a growth in length (Figure 5b–h), then in the *xy* plane (Figure 5i–n). This transition from 1D to 2D can be observed in the region of the current peak, which obviously includes all relevant events. Note here that the domains are now in a microscale range and do not disappear with increasing field, what reflects itself strongly in the hysteresis loop (Figure 1b). The total spontaneous polarization decreases drastically with every further repoling process at room temperature. As a consequence, the recorded current is much smaller than that of the first repoling process. The positive sign corresponds to the antiparallel polarization direction, which is represented here by the black regions inside the closed domains. In order to quantify the switching process, a moving domain wall is marked with a white arrow, pointing the moving direction in dependence of the applied field. The quantitative motion rate in the first repoling process is shown in Figure 3. The evaluation here is restricted to the first repoling process, because the domains are still distinguished from each other until the coercive field is reached. In the second repoling processes the domains build complex clusters. Thus no separated domains are available to evaluate in this phase.

Now, we analyze this complex structure more deeply by extracting the scanned volume at a certain field strength as before and compare it with the domain status in Figure 4. We chose the field point "n," at which E amounts to 3.5 kV cm^{-1}.

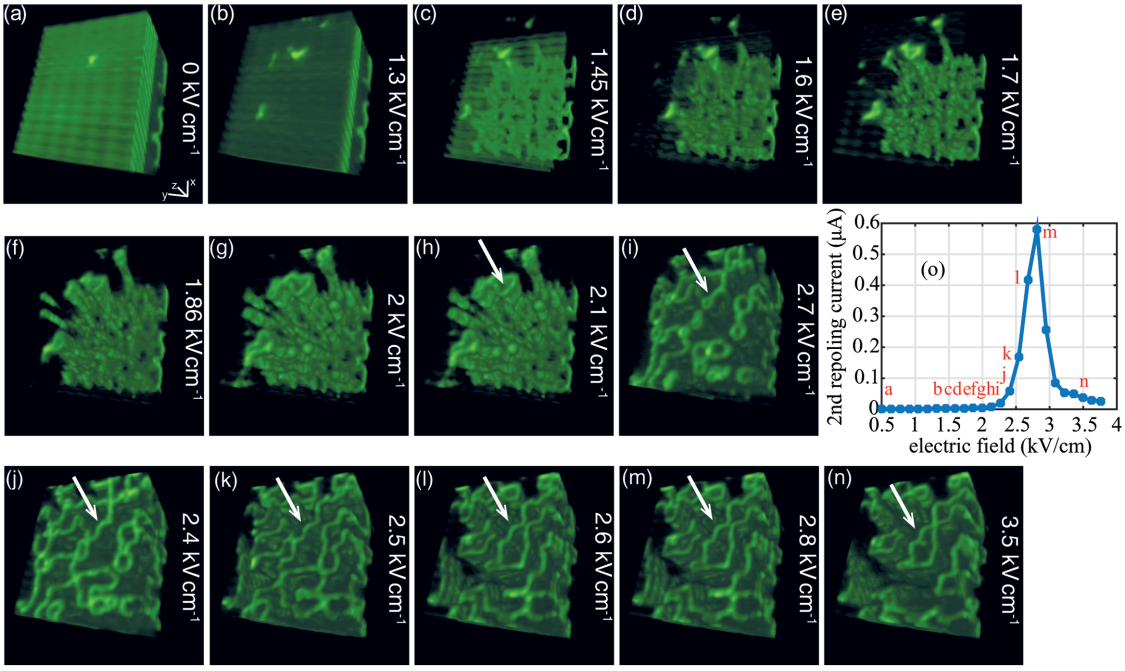

Figure 5. a–n) Measured 3D sequence of the second repoling process of a multidomain SBN crystal. The images are labeled on the corresponding transient current (o). The white arrow points to wall moving in one direction (see Video S2, Supporting Information). Green lines represent domain walls.

Adv. Mater. **2016**,
DOI: 10.1002/adma.201603325

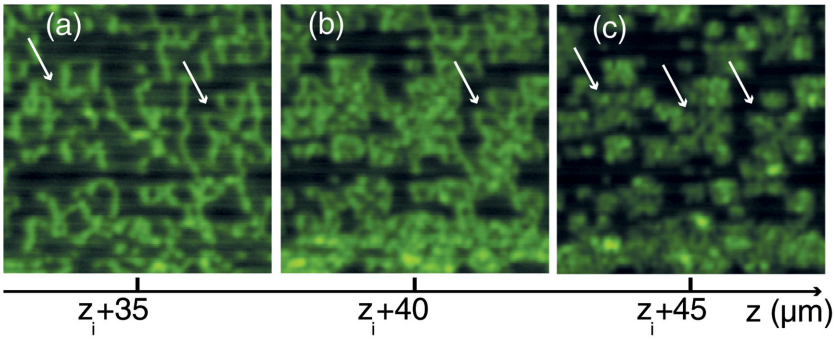

Figure 6. a–c) 2D images at different depths "z_i" extracted from the volume shown in Figure 5n at the field strength 3.5 kV cm^{-1} during the first repoling process. The domain roots are marked with white arrows. Green lines represent domain walls.

Figure 6 depicts the domain structures at different depths for this poling status. It shows again the individual symmetric domain "roots," filled with nanoscaled domains. This means, that the quadratic domains are now filled, with nanoscaled domains having a polarization antiparallel to those domains represented in the first repoling process (Figure 4). This indicates that after the switching process, the domains are not fully filled by an antiparallel domain, but rather with several nanoscaled domains, i.e., not completely switched. Consequently, less current flows and the hysteresis shrinks further.

Since the domains are large now we will show in the following which motion dimensionality will be dominant when performing the third repoling process.

Now, the course of the third repoling process is shown in **Figure 7** (see Video S3, Supporting Information). Here, we repole the fixed sample again starting from the last state of the second repoling process and record the current (Figure 7j). No noise signal is recorded in all layers due to the existence of the large domains. The electric field is increased in the same steps up to 1.7 kV cm^{-1}. No change in the form of the domain structures is observed and no current is recorded. By further increasing the field, domain walls start moving only laterally (Figure 7c). For distinguishing the motion direction in this process from the second repoling, the marked domain wall in Figure 5 will be further followed in Figure 7. The increasing field switches the domain by inducing a reversed wall motion (Figure 7b–f vs Figure 5i–n). One observes the growth of the spontaneous polarization, which is presented by the regions surrounded by domain walls. At about 2.8 kV cm^{-1}, the reversing process has finished. In comparison to the remaining structures after the second repoling process, much less structures are observed here, and the peak current is smaller. This can be attributed to the presence of an internal field caused by nonstoichiometric defects.[23,54,55] Moreover, the asymmetric behavior can clearly be seen as a shift in the current peak position for the three repoling processes. The peak positions determine the coercive field of the ferroelectric crystal, which is 3, 2.8, and 2.5 kV cm^{-1} for the three repoling processes, respectively.

The motion rates of the two switching directions of the marked wall shown in Figures 5 and 7 are depicted in **Figure 8**. The measurements show that the wall moves about 7 μm in the 2nd repoling process and about 3.5 μm in the 3rd repoling. The shift between both directions in the field values is clearly because of different repoling directions. This difference is consistent with the current measurements that show the aging effect. Thus in the third repoling process less current flows, what in turn indicates a decreased movement of the domain walls.

In conclusion, by using Čerenkov-type second-harmonic generation, we are able to visualize systematically one of the most complex dynamics of a relaxor multidomain ferroelectric in 3D with a submicrometer resolution. We identified the growth and the switching process of the ferroelectric domains in randomized strontium barium niobate in combination with the transient current, from which the domain kinetics can be extracted. The combination allowed us to assign every domain size statistic with its corresponding charge quantity, which is

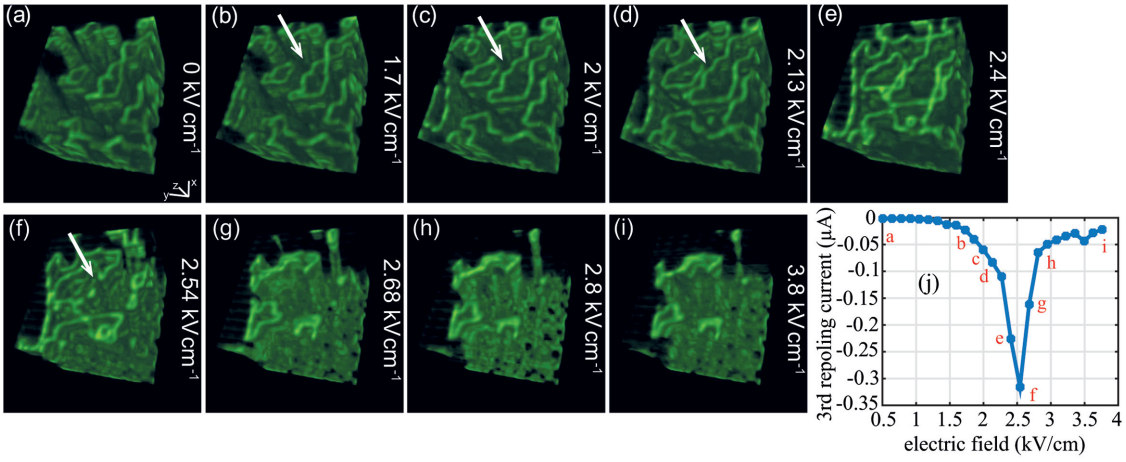

Figure 7. a–i) Measured 3D sequence of the third repoling process of a multidomain SBN crystal. The images are labeled on the corresponding transient current (o). The white arrow points to the same wall marked in Figure 5, yet moving in the other direction (see Video S3, Supporting Information). Green lines represent domain walls.

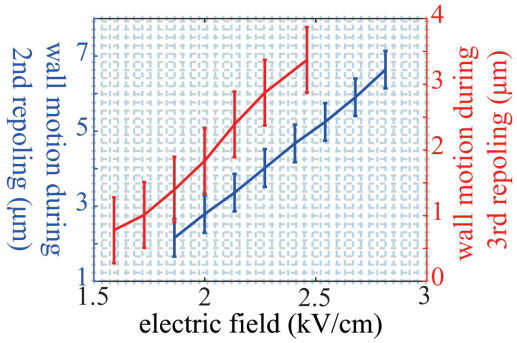

Figure 8. Comparison between the lateral domain wall motion rates in the 2nd repoling and 3rd repoling processes.

presented by the spontaneous polarization. Thus, it is possible to restore the desired averaged domain size by adjusting the spontaneous polarization without losing the disordered nature of the structures that is essential for many nonlinear optical processes. In addition, our results show the ability of exploring the domain formation process in dependence of any external parameters such as frequency of the electric field, temperature, or illumination by light.

Experimental Section

The optical setup (Figure 1a) mainly consisted of a commercial nonlinear laser scanning microscope (Nikon eclipse, Ti-U). The fundamental wave was generated by a Ti-Sapphire laser (Micra 5, Coherent), delivering pulses at 800 nm with 80 MHz repetition rate, 60 fs pulse duration, and up to 3.5 nJ pulse energy. The beam was coupled to the microscope and tightly focused by the microscope objective with a numerical aperture of 0.75 to a near diffraction limited spot in the sample. The position of the focus was raster scanned in all dimensions (layer by layer) with a piezo table (P-545, PI nano) in steps of 500 nm. Čerenkov SH signal was generated only at domain walls and no SH signal was generated in the homogeneous bulk of the sample. The intensity of the generated Čerenkov second-harmonic signal was collected by a condenser lens (0.9 NA) and recorded by a photomultiplier (H6780, Hamamatsu) as a function of the focus position. The fundamental beam was effectively blocked by using a proper filter.

The employed sample was a $Sr_{0.61}Ba_{0.39}Nb_2O_6$ with the dimensions $6 \times 6 \times 1.1$ mm^3 grown by the Czochralski method with a congruently melting composition $x = 0.61$ and doped with Cr_2O_3.[56] The large surfaces perpendicular to the *c*-axis were polished to optical quality. In order to be able to apply an electric field and to measure the reversal current at the same time, the large surfaces were coated with a 200 nm thick ITO film. It allowed carrying out the scan procedure while applying an external electric field and visualizing the ferroelectric domain dynamics quasi-live beginning from the nucleation process. In the experiment, the initial poling state of the sample was reset to avoid any differences between the total polarization states from an as-grown sample to another one, by heating it to ≈250 °C above the Curie-temperature ($T_c \approx 70$ °C) for 2 h. This was then followed by cooling it down without applying an electric field erasing any spurious polarization. The consecutive switching processes were expected to be differently pronounced. At first the nucleation took place, followed by a longitudinally and then sideways domain growth. Therefore, it was distinguished systematically between four defined poling states (Figure 1b), in which the events occurred: *field-cooled* state, where the crystal was heated up above the Curie temperature and cooled down to room temperature with an applied electric field. In this state the sample was a single-domain crystal. This was not considered in context of this paper. Second, the unpoled state, where the crystal was cooled down without an applied field. In this state the sample was similar to an as-grown crystal, i.e., multidomain crystal with nanoscaled domains.[49] Third, the state, where the crystal was poled at room temperature by applying an electric field above the coercive field. Fourth, the repoled state, where an unpoled crystal was first poled at room temperature and then repoled by applying a negative electric field above the coercive field, which was about 2.7 kV cm^{-1}, depending on the crystal composition and doping. In this case the crystal had a random distribution of microscaled 3D domains (Figure 1c). The green lines represented domain walls, i.e., they separated regions of opposite polarization directions either upward or downward. The polarization under the green pyramids (needles) in Figure 1c pointed in one direction along the *c*-axis and the polarization outside the pyramids pointed in the opposite direction. It was noted here that the poling at room temperature did not lead to a perfectly poled crystal unlike to the field-cooled case due to so-called aging effect.[52,57] An example of the influence of the aging on these 3D Domains was depicted in Figure 1d. Figure 1d shows 3D Čerenkov microscopic images of SBN needle-like domains after one and three repoling processes. It can be seen that the aging prevented the domain wall motion from closing the top of domains in order to form needle domains after three repoling cycles.

For profiling these 3D objects information in the depth was needed. The task was now to explore and analyze how these 3D objects grew to ultimately take their characteristic form. For this aim, three repoling processes were performed and the dynamics starting from the nucleation was imaged. The experimental procedure offered large datasets providing the possibility to explore and analyze every detail at each level in each depth. The lateral and longitudinal domain wall motion was analyzed in dependence of the applied electrical field quantitatively.

Supporting Information

Supporting Information is available from the Wiley Online Library or from the author.

Received: June 24, 2016
Revised: September 11, 2016
Published online:

[1] Y.-H. Shin, I. Grinberg, I.-W. Chen, A. M. Rappe, *Nature* **2007**, *449*, 881.
[2] L. E. Cross, *Ferroelectrics* **1987**, *76*, 241.
[3] D. Viehland, S. J. Jang, L. E. Cross, M. Wuttig, *J. Appl. Lett.* **1990**, *68*, 2916.
[4] V. Westphal, W. Kleemann, *Phys. Rev. Lett.* **1992**, *68*, 847.
[5] L. E. Cross, *Ferroelectrics* **1994**, *151*, 305.
[6] H. Rieger, *Phys. Rev. B* **1995**, *52*, 6659.
[7] R. Blinc, J. Dolinsek, A. Gregorovic, B. Zalar, C. Filipic, Z. Kutnjak, A. Levstik, R. Pirc, *Phys. Rev. Lett.* **1999**, *83*, 424.
[8] B. E. Vugmeister, H. Rabitz, *Phys. Rev. B* **2001**, *65*, 024111.
[9] W. Kleemann, J. Dec, P. Lehnen, R. Blinc, B. Zalar, R. Pankrath, *Eur. Phys. Lett.* **2002**, *57*, 14.
[10] T. Granzow, U. Dörfler, T. Woike, M. Wöhlecke, R. Pankrath, M. Imlau, W. Kleemann, *Europhys. Lett.* **2002**, *57*, 597.
[11] T. Granzow, T. Woike, M. Wöhlecke, M. Imlau, W. Kleemann, *Phys. Rev. Lett.* **2004**, *92*, 065701.
[12] K. Nassau, H. J. Levinstein, G. M. Loiacono, *Appl. Phys. Lett.* **1965**, *6*, 228.
[13] M. Houe, P. D. Townsend, *J. Phys. D: Appl. Phys.* **1995**, *28*, 1747.
[14] M. C. Wengler, M. Müller, E. Soergel, K. Buse, *Appl. Phys. B* **2003**, *76*, 393.

[15] T. J. Yang, V. Gopalan, P. J. Swart, U. Mohideen, *Phys. Rev. Lett.* **1999**, *82*, 4106.
[16] V. Gopalan, T. E. Mitchell, *J. Appl. Phys.* **1999**, *85*, 2304.
[17] M. Müller, E. Soergel, K. Buse, *Opt. Lett.* **2003**, *28*, 2515.
[18] M. Flörsheimer, R. Paschotta, U. Kubitscheck, C. Brillert, D. Hofmann, L. Heuer, G. Schreiber, C. Verbeek, W. Sohler, H. Fuchs, *Appl. Phys. B* **1998**, *67*, 593.
[19] G. Berth, W. Hahn, V. Wiedemeier, A. Zrenner, S. Sanna, W. G. Schmidt, *Ferroelectrics* **2011**, *420*, 44.
[20] S.-C. Pei, T.-S. Ho, C.-C. Tsai, T.-H. Chen, Y. Ho, P.-L. Huang, A. H. Kung, S.-L. Huang, *Opt. Express* **2011**, *19*, 7153.
[21] Y. Zhang, J. Wen, S. N. Zhu, M. Xiao, *Phys. Rev. Lett.* **2010**, *104*, 183901.
[22] Y. Uesu, S. Kurimura, Y. Yamamoto, *Ferroelectrics* **1997**, *191*, 135.
[23] L. Tian, D. A. Scrymgeour, V. Gopalan, *J. Appl. Phys.* **2005**, *97*, 114111.
[24] J. Kaneshiro, Y. Uesu, *Ferroelectrics* **2011**, *412*, 32.
[25] H. Yokota, J. Kaneshiro, Y. Uesu, *Phys. Res. Int.* **2012**, *2012*, 704634.
[26] Y. Sheng, A. Best, H.-J. Butt, W. Krolikowski, A. Arie, K. Koynov, *Opt. Express* **2010**, *18*, 16539.
[27] T. Kampfe, P. Reichenbach, M. Schroder, A. Hausmann, L. M. Eng, T. Woike, E. Soergel, *Phys. Rev. B* **2014**, *89*, 035314.
[28] W. J. Merz, *Phys. Rev.* **1954**, *95*, 690.
[29] V. Y. Shur, E. L. Rumyantsev, *Ferroelectrics* **1993**, *142*, 1.
[30] V. M. Fridkin, *Ferroelectrics* **2012**, *426*, 139.
[31] R. C. Miller, A. Savage, *Phys. Rev. Lett.* **1959**, *2*, 294.
[32] H. L. Stadler, P. J. Zachmanidis, *J. Appl. Phys.* **1963**, *34*, 3255.
[33] V. Y. Shur, E. L. Rumyantsev, *Ferroelectrics* **1994**, *151*, 171.
[34] R. L. Bihan, *Ferroelectrics* **1989**, *97*, 19.
[35] L. I. Dontzova, N. A. Tikhomirova, L. A. Shuvalov, *Ferroelectrics* **1989**, *97*, 87.
[36] C. D. Tran, X. Gerbaux, A. Hadni, *Ferroelectrics* **1981**, *33*, 31.
[37] B. D. Huey, R. Nath, *High-Speed Piezo Force Microscopy: Novel Observations Of Ferroelectric Domain Poling, Nucleation, and Growth* (Eds: S. V. Kalinin, A. Gruverman), Springer, New York **2011**, Ch. 11, p. 338.
[38] S. V. Kalinin, B. J. Rodriguez, S. Jesse, J. Shin, A. P. Baddorf, P. Gupta, H. Jain, D. B. Williams, A. Gruverman, *Microsc. Microanal.* **2006**, *12*, 206.
[39] R. Nath, S. Hong, J. A. Klug, A. Imre, M. J. Bedzyk, R. S. Katiyar, O. Auciello, *Appl. Phys. Lett.* **2010**, *96*, 163101.
[40] Y. Ishibashi, Y. Takagi, *J. Phys. Soc. Jpn.* **1971**, *31*, 506.
[41] A. R. Tunyagi, M. Ulex, K. Betzler, *Phys. Rev. Lett.* **2003**, *90*, 243901.
[42] S. M. Saltiel, Y. Sheng, N. Voloch-Bloch, D. N. Neshev, W. Krolikowski, A. Arie, K. Koynov, Y. S. Kivshar, *IEEE J. Quantum Electron.* **2009**, *45*, 1465.
[43] M. Ayoub, P. Roedig, J. Imbrock, C. Denz, *Appl. Phys. Lett.* **2011**, *99*, 241109.
[44] P. Karpinski, X. Chen, V. Shvedov, C. Hnatovsky, A. Grisard, E. Lallier, B. Luther-Davies, W. Krolikowski, Y. Sheng, *Opt. Express* **2015**, *23*, 14904.
[45] D. Viehland, Z. Xu, W.-H. Huang, *Philos. Mag. A* **1995**, *71*, 205.
[46] P. Lehnen, W. Kleemann, T. Woike, R. Pankrath, *Phys. Rev. B* **2001**, *64*, 224109.
[47] J. Dec, V. V. Shvartsman, W. Kleemann, *Appl. Phys. Lett.* **2006**, *89*, 212901.
[48] M. Ayoub, M. Paslick, K. Koynov, J. Imbrock, C. Denz, *Opt. Express* **2013**, *21*, 31462.
[49] P. Molina, M. de la O Ramírez, L. E. Bausá, *Adv. Funct. Mater.* **2008**, *18*, 709.
[50] V. V. Shvartsman, W. Kleemann, T. Lukasiewicz, J. Dec, *Phys. Rev. B* **2008**, *77*, 054105.
[51] V. Roppo, W. Wang, K. Kalinowski, Y. Kong, C. Cojocaru, J. Trull, R. Vilaseca, M. Scalora, W. Krolikowski, Y. Kivshar, *Opt. Express* **2010**, *18*, 4012.
[52] M. Ayoub, J. Imbrock, C. Denz, *Opt. Express* **2011**, *19*, 11340.
[53] J. Hatano, F. Suda, H. Futama, *Ferroelectrics* **1978**, *20*, 26.
[54] S. Kim, V. Gopalan, K. Kitamura, Y. Furukawa, *J. Appl. Phys.* **2001**, *90*, 2949.
[55] T. Volk, D. Isakov, M. S. Belsley, L. Ivleva, *Phys. Status Solidi A* **2009**, *2*, 321.
[56] K. Megumi, N. Nagatsuma, Y. Kashiwada, Y. Furuhata, *J. Mater. Sci.* **1976**, *11*, 1583.
[57] M. Ayoub, P. Roedig, K. Koynov, J. Imbrock, C. Denz, *Opt. Express* **2013**, *21*, 8220.